# **Inorganic Chemistry**

pubs.acs.org/IC Article

# Unsupported Lanthanide—Transition Metal Bonds: Ionic vs Polar Covalent?

Xin Yang, Corey P. Burns, Michael Nippe, and Michael B. Hall\*



Cite This: Inorg. Chem. 2021, 60, 9394-9401



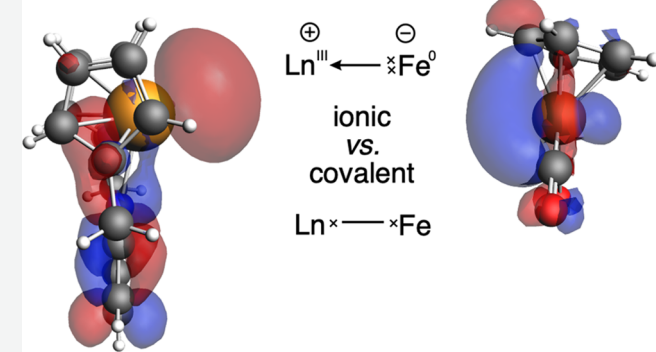
**ACCESS** 

Metrics & More

Article Recommendations

S Supporting Information

**ABSTRACT:** Lanthanide—transition metal complexes continue to be of interest, not only because of their synthetic challenge but also of their promising magnetic properties. Computational work examining the chemical bonding between lanthanides and transition metals in  $PyCp_2Ln-TMCp(CO)_2$  ( $DyPyCp_2^{2-} = [2,6-(CH_2C_5H_3)_2C_5H_3N]^{2-}$ ) reveals strong Ln-TM dative bonds. Gasphase optimized geometries are in good agreement with experimental structures at the density functional theory (DFT) level with large-core pseudopotentials. From La to Lu, there is a small increase in the bond dissociation energy, as well as a decrease in Ln-Fe bond lengths. Energy decomposition analyses attribute this trend to an increase in the electrostatic contribution from the decreasing bond length and a modest increase in the orbital



contribution. The natural bond orbital analysis clearly indicates that  $3d^6$  "lone pairs" in the  $[FeCp(CO)_2]^-$  fragment act as a Lewis bases donating nearly 0.5 electron to Ln virtual orbitals of mainly d character. The interfragment bonding was also quantified by the quantum theory of atoms in molecules, which indicates that the Ln–Fe bond is more covalent than the Ca–Fe bond in the hypothetical CpCa-Fe $Cp(CO)_2$  but less covalent than the Zn-Fe bond in the hypothetical CpZn-Fe $Cp(CO)_2$ . Further comparisons suggest that to the  $[PyCp_2Ln]^+$  cation the  $[FeCp(CO)_2]^-$  anion appears much like a halide. Overall, these Ln–TM dative bonds appear to have strong electrostatic contributions as well as significant orbital mixing and dispersion contributions.

#### ■ INTRODUCTION

Developing innovative types of metal-metal linkages has been fascinating scientists for many decades. 1-7 Recently, much effort has been devoted to understanding interactions between 4f-block elements and transition metals. 8,9 Owing to their significant synthetic challenge, examples of direct lanthanide to transition-metal bonds remain uncommon (Figure 1). Note that short distances between lanthanides and transition metals do not necessarily guarantee strong metal-metal bonds, such as the Lu-Pd(0) complex (1), where metal atoms are held in close proximity by the bridging aminopyridinato ligands. 10 Nevertheless, examples of Nd-Rh/Pt (2), 11 Lu-Pt (3), 12 and Lu-Ni (4)13 bonds have been synthesized with bridging ligands. Notably, the Lu-Ni complex from Ramirez et al. was the first case of molecules containing direct Ln-TM interactions to exhibit catalytic reactivity. On the other hand, the first appearance of an unsupported Ln-TM bond dates back to 1993, when Beletskaya et al. reported the directly bonded complex  $[Cp_2(thf)Lu-RuCp(CO)_2]$  (5). <sup>14</sup> The Lu-Fe analogue was not isolated due to its limited stability. Later, Arnold et al. synthesized an unsupported Ln-Fe complex, [(L')(N'')Nd-FeCp $(CO)_2]_2$   $[L' = Bu^tNCH_2CH_2\{C-CC\}]_2$  $(NCSiMe_3CHNBu^t)$ ;  $N'' = N(SiMe_3)_2$  (6), via saltelimination reaction. This Nd-Fe complex was sufficiently stable to be isolated and structured with a Nd-Fe bond distance of 2.994 Å. Beginning in 2008, several bismetallocene  $[Cp_2Ln-ReCp_2]$  complexes (7) with unsupported La/Sm/Yb/Lu-Re bonds were successfully synthesized through alkane elimination reactions by Kempe and his co-workers. <sup>16–18</sup> Meanwhile, the same group published striking results on molecular intermetalloids  $[Ln(ReCp_2)_3]$  (Ln = Sm, Lu, and La) that contain lanthanoid metals solely bound to transition metals in a triangular arrangement (8).

Understanding novel types of metal—metal chemical bonds was always of great fundamental interest, but only a few computational studies have been dedicated to elucidating the nature of direct Ln–TM bonds. <sup>13,15,16,20,21</sup> Kempe and coworkers pioneered the evaluation of Ln–Re bonds of 7 at the density functional theory (DFT) level by means of the electron localizability indicator (ELI-D). They identified the interaction energy between the Ln and TM fragments as dominated by the electrostatic interaction, while the occurrence of disynaptic

Received: January 28, 2021 Published: June 14, 2021





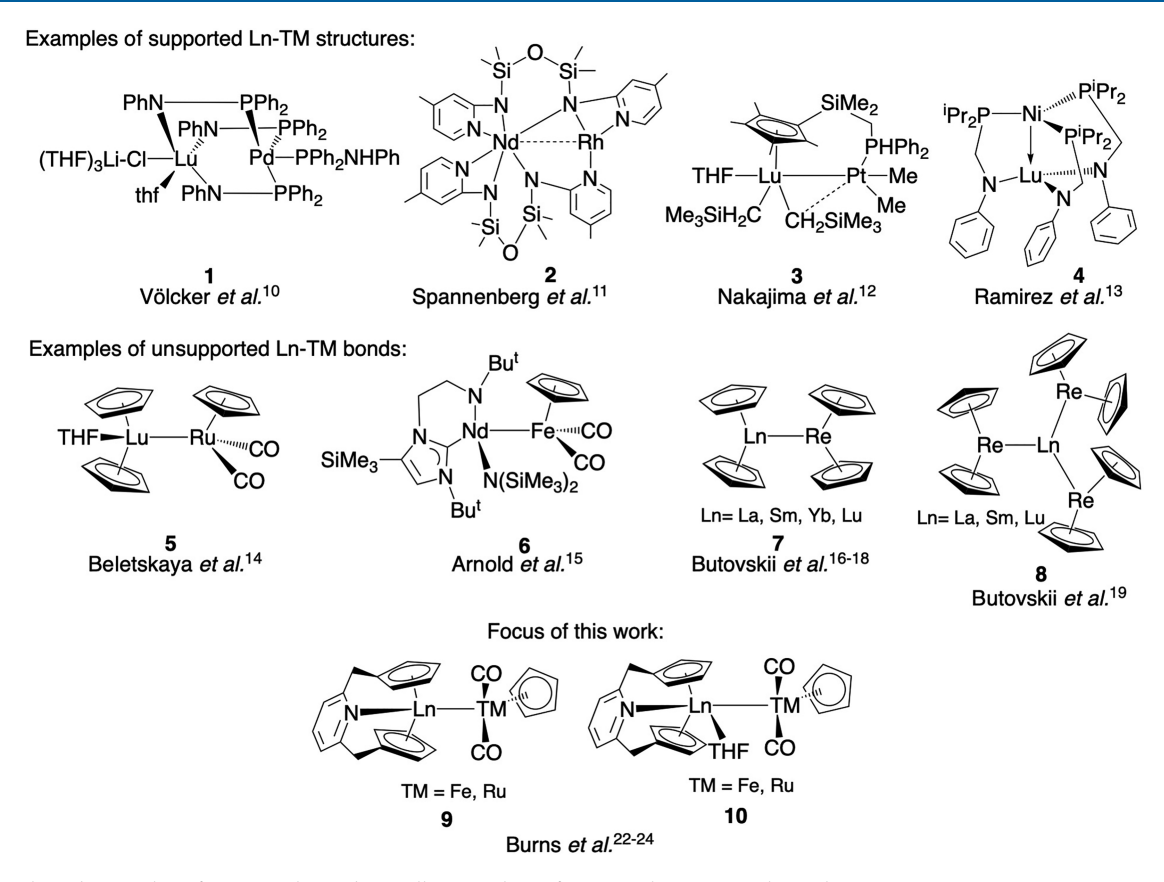


Figure 1. Selected examples of Ln-TM heterobimetallic complexes featuring the two metals in close proximity.

basins and distribution of basin population indicated "a characteristic covalent RE-TM bonding situation."20 On the other hand, research on the Nd-Fe amido N-heterocyclic carbene complex (6) suggested that the Nd-Fe interaction is "principally ionic" in character based on the natural bond orbital (NBO) analysis and calculated interaction energy of 384 kJ/mol between the {Fp}<sup>-</sup> and {Nd}<sup>+</sup> fragments. 15 Recently, complete active space self-consistent field (CASSCF) calculations on several An/Ln-M-bonded systems including [Cp<sub>2</sub>(thf)Lu-RuCp(CO)<sub>2</sub>] (5) indicated that the electronic structure of these systems is not multiconfigurational. Their results also suggested that An/Ln-M bonds are primarily ionic with  $\sigma$ -type donation from the metal ligand to the An/Ln fragment existing in all cases.<sup>21</sup> The differences in these bond descriptions are not irreconcilable as different analysis tools were used on different complexes. Thus, chemical bonds between lanthanides and transition metals are worth exploring in a uniform series of complexes with multiple characterization tools to provide a consistent and reliable interpretation of

In our previous communications, we reported characterization and analysis of  $PyCp_2Dy\text{-}TMCp(CO)_2$  (TM = Fe, Ru;  $PyCp_2^{2-} = [2,6\text{-}(CH_2C_5H_3)_2C_5H_3N]^{2-})$  and the (thf)Ce–Fe analogue from both experiment and theory. Since this ligand system is apparently capable of supporting other Ln–TM complexes, we investigated Ln to TM bonds in  $PyCp_2Ln\text{-}TMCp(CO)_2$  (TM = Fe, Ru) (9) with detailed theoretical analyses of the La–Fe, Dy–Fe, and Lu–Fe bonds. To distinguish the nature of these unconventional Ln–Fe bonds, comparisons are made with relevant analogues, for which the bonding characteristics are more generally accepted. A variety of analysis tools, such as NBO, topological analysis,

and energy decomposition analysis (EDA), are employed in this work. Given the general stability of these trivalent lanthanide compounds and the interest in their single-molecule magnetic properties, we hope this work will provide insight into the nature and periodic trends of Ln–TM bonding that will be helpful to future work on the properties of these systems. <sup>22,23</sup>

# EXPERIMENTAL SECTION (COMPUTATIONAL DETAILS)

Based on previous work, <sup>20</sup> the BP86<sup>25,26</sup> functional was selected for all of the DFT calculations of  $PyCp_2Ln-TMCp(CO)_2$  (TM = Fe, Ru) systems, and results for several other functionals are compared below. Geometry optimization and frequency calculations were performed with Gaussian 09, Revision D01<sup>27</sup> with the 6-311G\*<sup>28</sup> basis sets on C, H, O, and N atoms. The DFT wave functions were tested and confirmed to be stable. Large-core quasi-relativistic pseudopotentials were used for lanthanides (ECPnMWB, n = 46, 55, 60 for La, Dy,  $Lu^{29,30}$ ) in combination with their corresponding basis sets ((6s6p5d)/[4s4p4d] + 2s1p1d). The quasi-relativistic ECP28MWB was used on Ru, 33 and fully relativistic ECP10MDF on Fe,<sup>34</sup> with their respective valence basis set (Ru, (8s7p6d2f1g)/(6s5p3d2f1g); Fe, (8s7p6d2f1g)/(6s5p3d2f1g)). With this choice of ECP and basis set, all of the complexes are calculated as singlet states as the 4f electrons of Ln3+ are in its ECP. Solvation energies were calculated from gas-phase optimized geometries in tetrahydrofuran solvent (as was used in the experimental work) with the SMD<sup>36</sup> solvation model. Dispersion corrections were added to energies using the D3 version of Grimme's dispersion with the Becke-Johnson damping (GD3BJ).<sup>37</sup> The Kohn-Sham orbitals generated from gas-phase geometry optimizations were used for natural bond orbital analysis with NBO 6.0.3

Single-point calculations on both the large-core optimized geometries and available experimental structures were carried out

under the Douglas-Kroll-Hess (DKH)<sup>39</sup> second-order scalarrelativistic scheme, in combination with 6-311G\* for C, H, O, and N atoms as well as the all-electron correlation consistent basis sets for lanthanides (cc-pVTZ-DK3)40 and Fe (cc-pVTZ-DK).41 The allelectron DKH calculations produced electronic binding energies (BE) in excellent agreement with the ECP calculations (see Table S1). Topological analysis (the quantum theory of atoms in molecules, QTAIM<sup>42,43</sup>) was performed based on the Kohn-Sham orbitals generated from all-electron calculations by employing AIMAll.<sup>44</sup> For EDA calculations, geometry was optimized at the BP86/ZORA-TZ2P<sup>45</sup> (all-electron) level of theory followed by fragment analysis implemented in ADF2017.106.46,47 The ORCA 4.048 was also used for geometry optimization (BP86/SARC-ZORA-TZVP<sup>49</sup> on La, Dy, and Lu, old-ZORA-TZVP<sup>50</sup> on Ru, and ZORA-def2-TZVP<sup>51</sup> on others; integration grid was set to Grid7, NoFinalGrid) and generating wave function files for QTAIM analysis, leading to consistent results with Gaussian and ADF. Calculational methods on complexes other than PyCp<sub>2</sub>Ln-FeCp(CO)<sub>2</sub> are described in the SI.

#### ■ RESULTS AND DISCUSSION

**Geometry Optimization.** Geometry optimization (Figure 2) from BP86 with large-core ECP using G09 indicates that

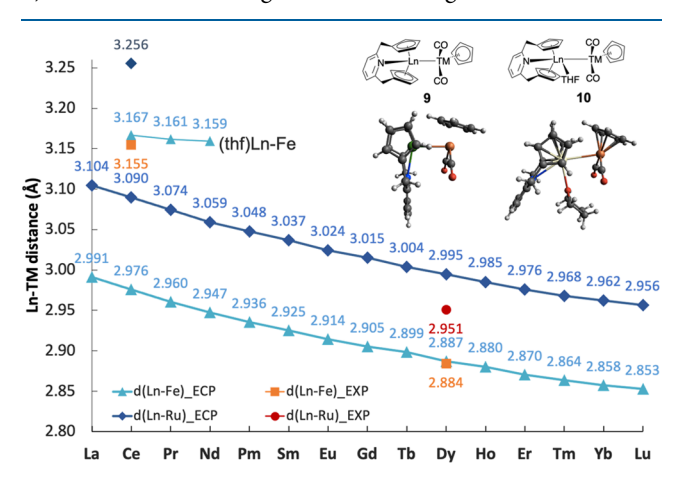
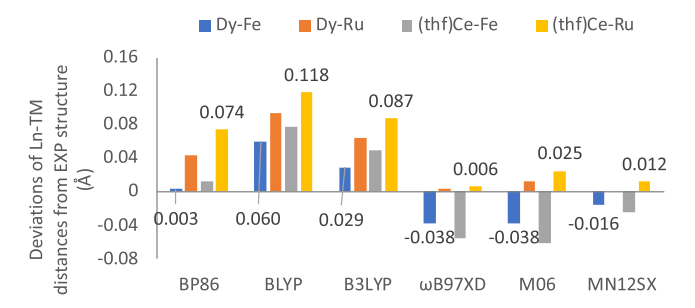


Figure 2. Bond lengths between lanthanide and iron/ruthenium in  $PyCp_2Ln-TMCp(CO)_2$  series of compounds from gas-phase-optimized structures calculated with large-core ECP for Ln (cyan/navy) show good agreement with several crystal structures (orange/red). Results of geometry optimization from scalar-relativistic all-electron calculations are discussed in the SI.

Ln–Fe and Ln–Ru bond distances decrease from La<sup>III</sup> 4f<sup>0</sup> to Lu<sup>III</sup> 4f, trends that are consistent with the change of Ln trivalent radii. Curstudies showed that tetrahydrofuran (thf) solvent molecules tend to coordinate to early lanthanides in the crystallization to form (thf)PyCp<sub>2</sub>Ln–TMCp(CO)<sub>2</sub> (Ln–TM = Ce–Ru, Ce–Fe, Pr–Fe, and Nd–Fe), and such coordination significantly elongates the Ln–TM bond distances. In this work, we will focus on the structures without coordinated tetrahydrofuran.

With regard to the choice of functionals for geometry optimization, the performance of BP86 was excellent for the Dy–Fe complex and the deviation from the experimental structure is only 0.003 Å. Bond length deviations calculated from several other functionals are also shown (Figure 3). Compared to BP86,  $^{25,26}$  the BLYP,  $^{25,53}$  and B3LYP  $^{53,54}$  functionals result in larger overestimations of the Dy/Ce–Fe bond lengths. These overestimations increase for ruthenium complexes, and this trend from Fe to Ru holds true for all tested functionals.  $\omega$ B97XD,  $^{55}$  M06,  $^{56}$  and MN12SX  $^{57}$  predict shorter bond lengths compared to the former three functionals,



**Figure 3.** Ln–TM bond length differences between DFT optimized geometries with selected functionals and experimental structures. Data labels are shown for Dy–Fe and (thf)Ce–Ru complexes.

causing an underestimation of iron complexes and providing more accurate results for ruthenium complexes. Although the MN12SX functional shows the least mean average error for these bond lengths, geometric differences are actually fairly small across functionals. Thus, we will continue to use the BP86 functional in this paper, especially since the focus is mainly on the Ln–Fe complexes. It is worthwhile to mention that BP86 optimized geometries with all-electron basis sets using ADF and ORCA are consistent (Table S2) with those from G09-ECP.

Since these complexes are synthesized from salt elimination of  $K[FeCp(CO)_2]$  and  $[PyCp_2Dy]OTf$  in THF (Scheme S1), a comparison of optimized bond lengths in the gas phase and in the solution, which parallels the experiment, can provide insight into the strength and polarity of the bonding interaction. In terms of BP86 gas-phase-optimized dysprosium complexes (ECP-G09), from Table 1, it is clear that dispersion shortens the Dy-Fe and -Ru bond distance by 0.07 and 0.08 Å, while solvation lengthened them by 0.19 and 0.10 Å, respectively. Hence, dispersion makes a strong contribution to shortening Ln-TM bonds, while implicit solvent effects have an even stronger effect on lengthening them. It is interesting that solvation elongated the Dy-Fe bond much more strongly than the Dy-Ru one. This latter result suggests that the bond is quite polar and fairly ionic as a weakly polar, covalent bond would not show such significant lengthening upon solvation.

Binding Energies. To calculate binding energies (BE), each Ln-Fe complex is split into two fragments by breaking the Ln-Fe bond. The intact complexes are optimized in the gas phase as described in the computational details. The values reported in the second column of Table 2,  $\Delta E_{\text{int GAS}}$ , are electronic interaction energies for the two fragments in their adduct ("frozen") geometries. The  $\Delta E_{\rm int~GAS}$  of two charged fragments in their frozen geometries,  $[PyCp_2Ln^{III}]^+$  and  $[CpFe^{0}(CO)_{2}]^{-}$ , are referred to as ionic  $\Delta E_{int\ GAS}$ , while the covalent  $\Delta E_{\text{int\_GAS}}$  were calculated from neutral fragments [PyCp<sub>2</sub>Ln<sup>II</sup>]<sup>0</sup> and [CpFe<sup>I</sup>(CO)<sub>2</sub>]<sup>0</sup>. For the rest of the columns, fragment geometries are fully optimized in the gas phase for meaningful values of the thermal corrections; hence, electronic binding energies,  $\Delta E_{\rm e\_GAS}$ , are slightly less negative than  $\Delta E_{\rm int\_GAS}$ . As expected, the ionic  $\Delta E_{\rm e\_GAS}$  values are much more negative than the covalent  $\Delta E_{\rm e~GAS}$  ones because of the large electrostatic interaction between charged species. Similar results for the binding energies were obtained when using crystal structures instead of optimized geometries and allelectron basis sets instead of large-core ECP (Table S3).

While electrostatics dominate ionic  $\Delta E_{\rm e\_GAS}$  values, as well as the enthalpy,  $\Delta H_{\rm GAS}$ , and Gibbs free energy,  $\Delta G_{\rm GAS}$ , for ionic fragments, ionic Gibbs free binding energies with solvent

Table 1. Comparison of Dy-Fe/Ru Bond Lengths (Å) Optimized with Different Methods

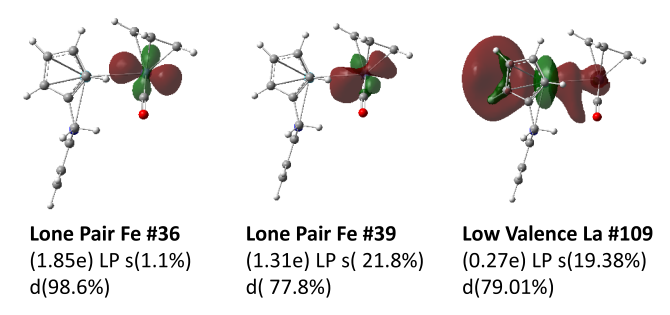
species	EXP	ECP-G09	ECP + disp.	ECP + SMD	ECP + disp. + SMD
Dy-Fe	2.883	2.887	2.819	3.078	2.994
Dy-Ru	2.951	2.995	2.916	3.097	3.024

Table 2. Gas-Phase Ionic and Covalent Interaction Energies ( $\Delta E_{\rm int\_GAS}$ , Frozen Fragment), Binding Electronic Energies ( $\Delta E_{\rm e\_GAS}$ ), Enthalpies ( $\Delta H_{\rm GAS}$ ), Gibbs Free Energies ( $\Delta G_{\rm GAS}$ ), Solvent-Corrected Gibbs Free Energies ( $\Delta G_{\rm SMD}$ ), and Solvent-Corrected Gibbs Free Energies with Dispersion Correction ( $\Delta G_{\rm SMD}$  + Disp.) of PyCp<sub>2</sub>La-FeCp(CO)<sub>2</sub>, PyCp<sub>2</sub>Dy-FeCp(CO)<sub>2</sub>, and PyCp<sub>2</sub>Lu-FeCp(CO)<sub>2</sub> from Gas-Phase Geometries and Fragments with G09

BE	$\Delta E_{ m int\_GAS}$	$\Delta E_{ m e\_GAS}$	$\Delta H_{ m GAS}$	$\Delta G_{ ext{GAS}}$	$\Delta G_{ m SMD}$	$\Delta G_{\rm SMD}$ + disp.
$[La]^+$ – $[Fe]^-$ ions	-122.8	-117.7	-116.0	-102.0	-4.4	-23.0
$[Dy]^+$ – $[Fe]^-$ ions	-126.7	-118.7	-116.8	-101.5	-7.3	-28.4
$[Lu]^+$ – $[Fe]^-$ ions	-128.7	-117.8	-115.7	-99.8	-11.5	-33.2
[La] <sup>0</sup> -[Fe] <sup>0</sup> neu	-59.4	-50.8	-48.4	-35.0	-28.6	-47.2
[Dy] <sup>0</sup> -[Fe] <sup>0</sup> neu	-62.1	-51.1	-48.2	-33.6	-23.1	-44.0
[Lu] <sup>0</sup> -[Fe] <sup>0</sup> neu	-62.7	-50.9	-47.9	-33.3	-25.9	-50.4

corrections,  $\Delta G_{\rm SMD}$ , are much smaller because of the stabilization of the free ions in solution. Neutral fragments are also stabilized by solvent corrections, to a less degree, as expected. Because ionic fragments are more stable in solution than the neutral ones, these complexes would dissociate into ions in solution. Dispersion contributes ca. 20 kcal/mol to both ionic and covalent  $\Delta E_{\rm e\_GAS}$ , suggesting noncovalent interactions also play an important role in stabilizing these complexes. It is remarkable to notice that the dispersion constitutes over half of the free energy of binding in solution.

Natural Bond Orbital Analysis. While it is obvious that substantial ionic interaction contributes to the bonding of these systems, there are orbital interactions, such as charge transfer (CT), that cannot be overlooked. The natural bond orbital (NBO) analysis performed on the La–Fe gas-phase-optimized geometry reveals an overall transfer of 0.48 electron from [CpFe(CO)<sub>2</sub>]<sup>-</sup> to [PyCp<sub>2</sub>La]<sup>+</sup> (0.50 electron from [CpFe(CO)<sub>2</sub>]<sup>-</sup> to [PyCp<sub>2</sub>Lu]<sup>+</sup>). The main interacting orbitals contributing to La–Fe bonding from second-order perturbation theory analysis and the number of electrons donated are shown in Figure 4. A large proportion of the orbital interaction



**Figure 4.** Selected natural bond orbitals (NBOs) of PyCp<sub>2</sub>La-FeCp(CO)<sub>2</sub>.

and charge transfer emerges from two Fe "lone pairs" of mainly 3d character donating to La "low-valence" and "Rydberg" orbitals. Among these interactions, the strongest (based on the off-diagonal Fock matrix element = 0.42 au) is between Fe 3d lone pair #39 and La #109 (Figure 4). A second relatively strong interaction (0.17 au) occurs with a different orientation between Fe d 3d lone pair #36 and La #109. The La #109 orbital accepts 0.27 e from these two Fe lone pairs and the rest of the electron density from the Fe fragment goes into a

number of other low valence accepting La orbitals (Figure S1) that are also mostly of d character. In terms of natural charges, donor-acceptor NBOs characteristics, and associated stabilization energies, the difference between La—Fe and Lu—Fe bonds is modest. Detailed results of NBO analysis on Lu—Fe are described in Figure S1 and Table S5.

Energy Decomposition Analysis. While the role of orbital mixing is addressed in the previous section, an in-depth analysis of other components of electronic interaction can be helpful. Inspired by the work of Frenking and co-workers, 58 an energy decomposition analysis (EDA) was performed on La-Fe and Lu-Fe complexes, where both close-shell charged fragments and open-shell neutral fragments were studied. In Table 3, the interaction energy  $\Delta E_e$  under the Mokokuma-type bond energy analysis<sup>59</sup> implemented in ADF comprises three components: the classical electrostatic interaction  $\Delta E_{\rm elst}$ , the Pauli repulsion  $\Delta E_{\text{Pauli}}$ , and the orbital interaction energy  $\Delta E_{\rm orb}$ . The ADF optimized bond distances (La-Fe, 2.996 Å; Lu-Fe, 2.838 Å) and total electronic interaction energies  $([La]^+-[Fe]^-, -119.7 \text{ kcal/mol}; [La]^0-[Fe]^0, -60.3 \text{ kcal/}$ mol; [Lu]<sup>+</sup>-[Fe]<sup>-</sup>, -125.2 kcal/mol; [Lu]<sup>0</sup>-[Fe]<sup>0</sup>, -59.7 kcal/mol) are consistent with the results from G09, above. For ionic fragmentation, electrostatic interactions make up ~75% of the total attractive contributions. The orbital interactions derived from ionic fragmentation are significantly smaller both in magnitude and in percentage than ones from neutral fragmentation. For neutral fragmentation, the attractive contributions are composed of nearly half electrostatic interaction and half orbital interaction. The neutral fragmentation of the Lu-Fe and La-Fe complexes results in similar magnitude of orbital interaction and total interaction energy, but quite different  $\Delta E_{\text{elst}}$  and  $\Delta E_{\text{Pauli}}$ . When one combines  $\Delta E_{\rm elst}$  and  $\Delta E_{\rm Pauli}$ , as a term to represent the interaction of fragments with antisymmetrized wave functions without electronic relaxation, the sum is comparable for Lu-Fe and La-Fe. The overall larger orbital interactions for the neutral fragments suggest that there is more charge transfer in the neutral fragments than in the charged ones. Thus, the EDA indicates that the fragments in the whole molecule are closer to ionic ones than neutral ones.

To further elucidate the chemical bonding in Ln–Fe systems, we computationally substituted the  $[FeCp(CO)_2]^-$  fragment with simpler anionic ligands:  $Cl^-$ ,  $Br^-$ , and  $I^-$ . As expected, the La-halide distance increases with the respective

Table 3. Results of the EDA of  $PyCp_2La-FeCp(CO)_2$  and  $PyCp_2Lu-FeCp(CO)_2$  Complexes at the BP86/TZ2P with Scalar-Relativistic Correction

molecule	PyCp <sub>2</sub> La-I	$FeCp(CO)_2$	$PyCp_2Lu$ - $FeCp(CO)_2$		
	$[PyCp_2La]^+(S)$	$[PyCp_2La]^0$ (D)	[PyCp <sub>2</sub> Lu] <sup>+</sup> (S)	$[PyCp_2Lu]^0$ (D)	
fragments	$[CpFe(CO)_2]^-(S)$	$[CpFe(CO)_2]^0$ (D)	$[CpFe(CO)_2]^-(S)$	$[CpFe(CO)_2]^0$ (D)	
$\Delta E_{ m int}$	-119.7	-60.3	-125.2	-59.7	
$\Delta E_{ m Pauli}$	82.5	84.2	85.4	156.0	
$\Delta E_{ m elst}{}^a$	-150.5 (74.4%)	-59.1 (40.9%)	-155.4 (74.0%)	-120.2 (55.8%)	
$\Delta E_{ m orb}^{a}$	-51.8 (25.6%)	-85.3 (59.1%)	-54.9 (24.0%)	-95.4 (44.2%)	

<sup>&</sup>lt;sup>a</sup>The percentage in parentheses is the % that a contribution makes to the total attractive contributions.

Table 4. Results of Energy Decomposition Analysis (EDA) from ADF Using Ionic Fragments (Energies in kcal/mol)

kcal/mol	d (Å)	$\Delta E_{ m int}$	$\Delta E_{ m Pauli}$	$\Delta E_{ m elst}$	$\Delta E_{ m orb}$	% elst <sup>a</sup>	% orb <sup>a</sup>
La-Fe	2.996	-119.7	82.5	-150.5	-51.8	74.4	25.6
Lu-Fe	2.859	-125.2	85.4	-155.4	-54.9	74.0	26.0
La-Cl	2.669	-136.7	75.2	-158.1	-53.8	74.6	25.4
La-Br	2.833	-127.7	72.3	-149.6	-50.4	74.8	25.2
La-I	3.083	-117.1	62.5	-135.1	-44.5	75.2	24.8
Lu-I	2.897	-121.6	72.0	-145.1	-48.5	74.9	25.1
Ca-Fe	2.747	-140.0	54.6	-149.8	-44.8	77.0	23.0
Zn-Fe	2.353	-209.5	81.5	-187.5	-103.6	64.6	35.6

<sup>&</sup>lt;sup>a</sup>These are the % that each contribution makes to the total attractive contributions.

halide size. The EDA analysis shows that all of the halide substitution analogues produce results exceedingly similar to ionic fragmentation of Ln-Fe ones in terms of the ratio of electrostatic interactions versus orbital interactions. Among the halide complexes, Ln-I analogues are the closest to Ln-Fe in terms of bond lengths and total interaction energies, except that Ln-I bonds are slightly longer and more polar (with more electrostatic interaction) than Ln-Fe bonds. Combined with the NBO analysis in the previous section, when bonding with  $[PyCp_2Ln]^+$ ,  $[CpFe(CO)_2]^-$  acts like an  $I^-$  by presenting lone pairs to the unoccupied orbitals in the Ln fragment with a strong ionic contribution and significant orbital mixing. In a second comparison, the [PyCp<sub>2</sub>Ln]<sup>+</sup> fragment was replaced by [CpCa]<sup>+</sup> and [CpZn]<sup>+</sup>, which were chosen as examples of closed-shell metallo-cations with empty and filled 3d orbitals, to create hypothetical model systems abbreviated as Ca-Fe, Zn-Fe in Table 4. The Ca-Fe complex has a shorter intermetallic bond distance than Ln-Fe complexes and the highest percentage of electrostatic interaction (77.0%) in Table 4. Alternatively, the Zn-Fe complex has the least percentage of electrostatic interaction (64.6%), despite having the largest electrostatic energy component and overall interaction energy among all of the molecules in Table 4, a difference due in part to its shorter bond. Thus, in terms of the ionic fragmentation scheme, the Ln-Fe bond looks more like Ln-I and Ca-Fe, while Zn-Fe is much more covalent than the rest of the bonds in Table 4. Additional EDA results for neutral fragments are provided in Table S4.

Quantum Theory of Atoms in Molecule Analysis. Analysis of electron density in intact molecules serves as an alternative way to characterize bonding with the advantage of avoiding artificially splitting the complex into two somewhat arbitrary fragments. Thus, the quantum theory of atoms in molecule (QTAIM) analysis was applied to the Ln–TM complexes and their analogues. In QTAIM, neighboring atoms (atomic basins) are delineated by what is known as interatomic surface (Figure 5) where there is no flux in the gradient vector field of electron density  $\nabla \rho$  through the surface, a point at

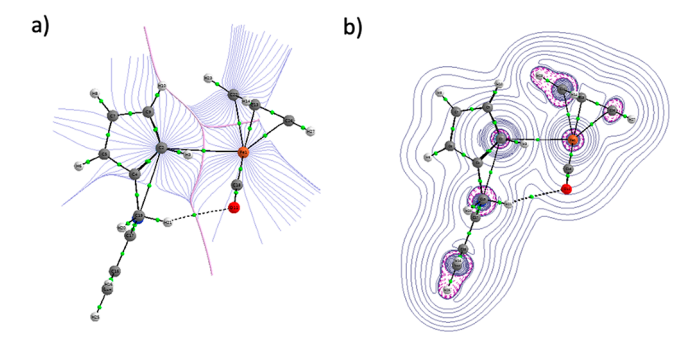


Figure 5. Illustration of (a) basin paths with interatomic surface and (b) contour plots of  $\nabla^2 \rho$  on the La–Fe–C(Cp) plane from QTAIM analysis.

which  $\nabla \rho = 0$  is called a critical point. For every pair of neighboring atoms, a critical point is found in the interatomic surface perpendicular to the internuclear axis. At this point, the density is a minimum along the line of the nuclei and a maximum with respect to the directions perpendicular to this line. This point has been referred to as bond critical point, though we prefer line critical point (lcp) as Shahbazian suggested<sup>60</sup> because the existence of this point should not be interpreted as indicating a chemical bond. Other QTAIM properties such as values of the density, the Laplacian of the density, and energy densities at the lcp are characteristics of the nature of the interaction. In a classical covalent bond, both the Laplacian,  $\nabla^2 \rho(\text{lcp})$ , and total energy density, H(lcp), are negative. In an ionic bond, both are positive. A less clear case occurs when  $\nabla^2 \rho(\text{lcp}) > 0$  and H(lcp) < 0; such interactions fall into the category of intermediate interactions like dative bonds.21

The QTAIM properties of these complexes are relatively unaffected by the choice of functionals, as demonstrated in Table S6. Results from BP86 calculations were shown here for analysis (Table 5). In entire series of complexes, the electron density,  $\rho(lcp)$ , and the Laplacian of the density,  $\nabla^2 \rho(lcp)$ ,

Table 5. Bond Distance (in Å) and QTAIM Properties (in au)<sup>a</sup>

A-B	d (A–B) Å	$\rho(\text{lcp})$	$ abla^2  ho(\mathrm{lcp})$	H(lcp)	DI(A,B)	$CT^e$
La-Fe <sup>b</sup>	2.991	0.036	0.044	-0.007	0.403	0.31
Dy-Fe <sup>c</sup>	2.884	0.036	0.047	-0.007	0.447	0.36
Lu−Fe <sup>c</sup>	2.838	0.037	0.047	-0.008	0.336	0.31
La-Cl	2.690	0.056	0.123	-0.010	0.624	0.27
La-Br	2.864	0.047	0.090	-0.008	0.611	0.28
La-I <sup>d</sup>	3.102	0.039	0.061	-0.006	0.603	0.30
Dy-I <sup>d</sup>	2.973	0.041	0.072	-0.007	0.609	0.33
Lu–I <sup>d</sup>	2.925	0.042	0.073	-0.008	0.525	0.31
Ca-Fe <sup>d</sup>	2.745	0.033	0.070	-0.005	0.282	0.23
Zn-Fe <sup>d</sup>	2.349	0.062	0.080	-0.018	0.702	0.83
_						

<sup>a</sup>CT, charge transfer between two fragments cleaved along A–B. <sup>b</sup>Optimized geometry. <sup>c</sup>Experimental geometry. <sup>d</sup>Optimized geometry (detailed computational methods are described in the SI). <sup>c</sup>Charge transfer: one minus the sum of the basin charge for fragment A.

have small positive values, while the total energy density, H(lcp), has small negative values in these cases. Thus, all of these chemical interactions fall into the category of intermediate interactions. The most ionic and least ionic species identified by the EDA analysis, Ca-Fe and Zn-Fe, also set the limits for  $\rho(lcp)$  and H(lcp) despite their similar intermediate  $\nabla^2 \rho(\text{lcp})$  values. Examination of geometric and QTAIM properties evinced that as the La-X distances increase from Cl to I,  $\rho(lcp)$ ,  $\nabla^2 \rho(lcp)$ , and negativity of H(lcp)decrease. A related trend with a much smaller range exists for the Ln series of La-I, Dy-I, and Lu-I; in the Ln series, the trend has the same relation between bond lengths and QTAIM properties. Overall it would seem that QTAIM also indicates that Ln-Fe bonds are more covalent than Ca-Fe but less covalent than Zn-Fe, while with respect to halides, Ln-Fe bonds are most similar to Ln-I bonds. In addition to the traditional ionic and covalent bonding scheme, one might consider whether charge-shift bonding (CSB) makes a contribution to these complexes. 61-64 From the prospective of QTAIM, features that make CSB different than those of either covalent or ionic are significant density and high positive Laplacian of the density at the line critical point.<sup>64</sup> The QTAIM properties of the studied Ln-Fe bonds (Table 5) do not support significant contributions from CSB.

In addition to QTAIM properties at the lcp, delocalization index (DI) was also employed to measure the extent to which the electrons in atom A are delocalized into atom B and vice versa. According to Bader, the primary developer of QTAIM, and his co-workers, DI provides a quantitative measure of the sharing of electrons between A and B, but it is not identified with a bond order.  $^{65}$  Only in nonpolar interactions like  $H_2$  and  $N_2$  (DI (H,H) = 1.000 and DI (N,N) = 3.042 at Hartree-Fock level), will the DI equate to the corresponding number of contributing Lewis-bonded pairs. At the other extreme, for example, DI of the generally acknowledged LiF ionic system equals 0.178, while for isoelectronic polar molecules NO+, CN<sup>-</sup>, and CO with an intermediate degree of charge transfer, DI values are 2.405, 2.210, and 1.574.65 The substantially smaller DI of CO arises from larger electronegativity difference in CO than in NO+ and CN-, which implies that DI strongly decreases as the polarity of the bond increases.

The DI values in Table 5 show that Ca—Fe has the smallest electron delocalization while Zn—Fe has the largest (Ca—Fe, 0.282; Zn—Fe, 0.702). These numbers that are in good

agreement with their difference in covalency implied by H(lcp). The DIs of Ln–Fe are between Ca–Fe and Zn–Fe, but closer to Ca–Fe, like other measures of their trend in covalency. The DI values of Ln halides are nearly constants, as one would expect from the similarity of the electrostatic ratio of La halides from the previous EDA, while they always have higher DIs than Ln–Fe, which reflects somewhat higher ionicity of Ln–Fe bonds compared to Ln halides.

Among the Ln series, the Dy–I shows higher DI than its La/Lu analogues, which is also true in Ln–Fe complexes. Unlike the periodic trends found in Ln–Fe distances, the DI of Dy–Fe (DI = 0.447) has the largest value among the three Ln–Fe species. The particularity of Dy–Fe is also evidenced by QTAIM basin atomic charges, where the interfragment charge transfer is among the highest in Ln–Fe (La, 0.31; Dy, 0.36; Lu, 0.31). The QTAIM results were further verified by wave functions generated from ADF (Table S7) and ORCA (Table S8).

#### CONCLUSIONS

DFT calculations using large-core ECP predict geometries in good agreement with the experimental ones. The magnitude of binding energies is highly subject to the definition of the fragments. Formation from the ions, [CpFe(CO)<sub>2</sub>]<sup>-</sup> to [PyCp<sub>2</sub>Ln]<sup>+</sup>, shows that 75% of the attractive interaction is electrostatic and 25% is orbital mixing, while neutral fragments produce binding energy of the same magnitude as the orbital mixing of the ions. Results from QTAIM and EDA indicated the Ln-Fe bonds are intermediate between Ca-Fe and Zn-Fe. Overall, they are very similar to Ln-I bonds with a modest difference across the series. Hence, we believe that the interactions of Ln-Fe are best described as dative bonds with strong electrostatic (ionic) contributions, as well as significant orbital mixing (electron delocalization, charge transfer, polarization), and dispersion contributions. This description appears to hold along the entire lanthanide series.

### ASSOCIATED CONTENT

#### Supporting Information

The Supporting Information is available free of charge at https://pubs.acs.org/doi/10.1021/acs.inorgchem.1c00285.

Overview of the synthesis of PyCp<sub>2</sub>Ln-TMCpCO<sub>2</sub>; computational details; gas-phase ionic and covalent binding energies (Table S1); Ln-Fe distances (in Å) from crystal and DFT optimized geometries structures (Table S2); ionic and covalent electronic binding energies (Table S3); supplementary results of energy decomposition analysis (Table S4); detailed results of NBO analysis (Table S5); additional QTAIM analysis of La-Fe and Lu-Fe (Table S6); QTAIM results from ADF (Table S7); QTAIM results from ORCA (Table S8); major interacting natural bond orbitals (Figure S1); additional La-Fe acceptor orbitals from NBO analysis (Figure S2); comparison of calculated Ln-Fe bond lengths (Figure S3); Mulliken atomic charge from ORCA scalar-relativistic all-electron calculations (Figure S4); difference between calculated spin density and ideal number of unpaired electrons (Figure S5); and difference between expectation values of  $S^2$  and exact values (Figure S6) (PDF)

xyz (ZIP)

### AUTHOR INFORMATION

## **Corresponding Author**

Michael B. Hall — Department of Chemistry, Texas A&M University, College Station, Texas 77845, United States; orcid.org/0000-0003-3263-3219; Email: mbhall@tamu.edu

#### **Authors**

Xin Yang — Department of Chemistry, Texas A&M University, College Station, Texas 77845, United States; ocid.org/0000-0003-0085-7859

Corey P. Burns — Department of Chemistry, Texas A&M University, College Station, Texas 77845, United States Michael Nippe — Department of Chemistry, Texas A&M University, College Station, Texas 77845, United States; orcid.org/0000-0003-1091-4677

Complete contact information is available at: https://pubs.acs.org/10.1021/acs.inorgchem.1c00285

#### Notes

The authors declare no competing financial interest.

#### ACKNOWLEDGMENTS

The authors are grateful for financial support from the National Science Foundation (CHE-1664866 and CHE-1753014) and the Robert A. Welch Foundation (A-0648 and A-1880). The authors acknowledge the Laboratory for Molecular Simulations and the High-Performance Research Computing Facility (http://hprc.tamu.edu/) for providing computing resources useful in conducting the research reported in this paper.

# **■ REFERENCES**

- (1) Albert Cotton, F.; Murillo, C. A.; Walton, R. A. *Multiple Bonds between Metal Atoms*; 3rd ed.; Springer Science and Business Media, New York, NY, 2005.
- (2) Bauer, J.; Braunschweig, H.; Dewhurst, R. D. Metal-Only Lewis Pairs with Transition Metal Lewis Bases. *Chem. Rev.* **2012**, *112*, 4329–4346.
- (3) Oelkers, B.; Kempe, R. Group 3, Lanthanide, and Actinide Metal–Metal Bonds. In *Molecular Metal-Metal Bonds*; John Wiley & Sons, Ltd., 2015; pp 47–71.
- (4) Berry, J. F.; Lu, C. C. Metal–Metal Bonds: From Fundamentals to Applications. *Inorg. Chem.* **2017**, *56*, 7577–7581.
- (5) Powers, I. G.; Uyeda, C. Metal-Metal Bonds in Catalysis. ACS Catal. 2017, 7, 936-958.
- (6) Duncan Lyngdoh, R. H.; Schaefer, H. F.; King, R. B. Metal—Metal (MM) Bond Distances and Bond Orders in Binuclear Metal Complexes of the First Row Transition Metals Titanium Through Zinc. Chem. Rev. 2018, 118, 11626—11706.
- (7) Chipman, J. A.; Berry, J. F. Paramagnetic Metal—Metal Bonded Heterometallic Complexes. *Chem. Rev.* **2020**, *120*, 2409–2447.
- (8) Liddle, S. T. Non-Traditional Ligands in f-Block Chemistry. *Proc. R. Soc. A* **2009**, 465, 1673–1700.
- (9) Oelkers, B.; Butovskii, M. V.; Kempe, R. F-Element-Metal Bonding and the Use of the Bond Polarity To Build Molecular Intermetalloids. *Chem. Eur. J.* **2012**, *18*, 13566–13579.
- (10) Völcker, F.; Mück, F. M.; Vogiatzis, K. D.; Fink, K.; Roesky, P. W. Bi- and Trimetallic Rare-Earth—Palladium Complexes Ligated by Phosphinoamides. *Chem. Commun.* **2015**, *51*, 11761—11764.
- (11) Spannenberg, A.; Oberthür, M.; Noss, H.; Tillack, A.; Arndt, P.; Kempe, R. Metal-Metal "Communication" of Rh or Pd with Nd in Novel Heterobinuclear Complexes. *Angew. Chem., Int. Ed.* **1998**, *37*, 2079–2082.

- (12) Nakajima, Y.; Hou, Z. Rare-Earth-Metal/Platinum Heterobinuclear Complexes Containing Reactive Ln-Alkyl Groups (Ln = Y, Lu): Synthesis, Structural Characterization, and Reactivity. *Organometallics* **2009**, *28*, 6861–6870.
- (13) Ramirez, B. L.; Sharma, P.; Eisenhart, R. J.; Gagliardi, L.; Lu, C. C. Bimetallic Nickel-Lutetium Complexes: Tuning the Properties and Catalytic Hydrogenation Activity of the Ni Site by Varying the Lu Coordination Environment. *Chem. Sci.* **2019**, *10*, 3375–3384.
- (14) Beletskaya, I. P.; Voskoboynikov, A. Z.; Chuklanova, E. B.; Kirillova, N. I.; Shestakova, A. K.; Parshina, I. N.; Gusev, A. I.; Magomedov, G. K. I. Bimetallic Lanthanide Complexes with Lanthanide-Transition Metal Bonds. Molecular Structure of (C4H8O)(C5H5)2LuRu(CO)2(C5H5). The Use of 139La NMR Spectroscopy. J. Am. Chem. Soc. 1993, 115, 3156–3166.
- (15) Arnold, P. L.; McMaster, J.; Liddle, S. T. An Unsupported Transition Metal—Lanthanide Bond; Synthesis and Crystal Structure of an Nd–Fe Amido N-Heterocyclic Carbene Complex. *Chem. Commun.* **2009**, *7*, 818–820.
- (16) Butovskii, M. V.; Tok, O. L.; Wagner, F. R.; Kempe, R. Bismetallocenes: Lanthanoid-Transition-Metal Bonds through Alkane Elimination. *Angew. Chem., Int. Ed.* **2008**, *47*, 6469–6472.
- (17) Döring, C.; Dietel, A.-M.; Butovskii, M. V.; Bezugly, V.; Wagner, F. R.; Kempe, R. Molecular [Yb(TM)2] Intermetalloids (TM=Ru, Re). *Chem. Eur. J.* **2010**, *16*, 10679–10683.
- (18) Butovskii, M. V.; Tok, O. L.; Bezugly, V.; Wagner, F. R.; Kempe, R. Molecular Lanthanoid—Transition-Metal Cluster through C-H Bond Activation by Polar Metal—Metal Bonds. *Angew. Chem., Int. Ed.* **2011**, *50*, 7695—7698.
- (19) Butovskii, M. V.; Döring, C.; Bezugly, V.; Wagner, F. R.; Grin, Y.; Kempe, R. Molecules Containing Rare-Earth Atoms Solely Bonded by Transition Metals. *Nat. Chem.* **2010**, *2*, 741–744.
- (20) Butovskii, M. V.; Oelkers, B.; Bauer, T.; Bakker, J. M.; Bezugly, V.; Wagner, F. R.; Kempe, R. Lanthanoid-Transition-Metal Bonding in Bismetallocenes. *Chem. Eur. J.* **2014**, *20*, 2804–2811.
- (21) Vlaisavljevich, B.; Miro, P.; Cramer, C. J.; Gagliardi, L.; Infante, I.; Liddle, S. T. On the Nature of Actinide- and Lanthanide-Metal Bonds in Heterobimetallic Compounds. *Chem. Eur. J.* **2011**, *17*, 8424–8433.
- (22) Burns, C. P.; Yang, X.; Wofford, J. D.; Bhuvanesh, N. S.; Hall, M. B.; Nippe, M. Structure and Magnetization Dynamics of Dy–Fe and Dy–Ru Bonded Complexes. *Angew. Chem., Int. Ed.* **2018**, *57*, 8144–8148.
- (23) Burns, C. P.; Yang, X.; Sung, S.; Wofford, J. D.; Bhuvanesh, N. S.; Hall, M. B.; Nippe, M. Towards Understanding of Lanthanide—Transition Metal Bonding: Investigations of the First Ce—Fe Bonded Complex. *Chem. Commun.* **2018**, *54*, 10893—10896.
- (24) Burns, Corey P. Complexes Containing a Direct, Unsupported Lanthanide-Transition Metal Bond. Doctoral Dissertation, Texas A&M University, 2019.
- (25) Becke, A. D. Density-Functional Exchange-Energy Approximation with Correct Asymptotic Behavior. *Phys. Rev. A* **1988**, *38*, 3098–3100.
- (26) Perdew, J. P. Density-Functional Approximation for the Correlation Energy of the Inhomogeneous Electron Gas. *Phys. Rev.* B 1986, 33, 8822–8824.
- (27) Frisch, M. J. et al.et al. Gaussian 09, revision D.01, Gaussian Inc., Wallingford CT, 2009.
- (28) Krishnan, R.; Binkley, J. S.; Seeger, R.; Pople, J. A. Self-consistent Molecular Orbital Methods. XX. A Basis Set for Correlated Wave Functions. *J. Chem. Phys.* **1980**, *72*, 650–654.
- (29) Dolg, M.; Stoll, H.; Savin, A.; Preuss, H. Energy-Adjusted Pseudopotentials for the Rare Earth Elements. *Theor. Chim. Acta* **1989**, 75, 173–194.
- (30) Dolg, M.; Stoll, H.; Preuss, H. A. A Combination of Quasirelativistic Pseudopotential and Ligand Field Calculations for Lanthanoid Compounds. *Theor. Chim. Acta* **1993**, *85*, 441–450.
- (31) Yang, J.; Dolg, M. Valence Basis Sets for Lanthanide 4f-in-Core Pseudopotentials Adapted for Crystal Orbital Ab Initio Calculations. *Theor. Chem. Acc.* **2005**, *113*, 212–224.

- (32) Weigand, A.; Cao, X.; Yang, J.; Dolg, M. Quasirelativistic F-in-Core Pseudopotentials and Core-Polarization Potentials for Trivalent Actinides and Lanthanides: Molecular Test for Trifluorides. *Theor. Chem. Acc.* **2010**, *126*, 117–127.
- (33) Andrae, D.; Häußermann, U.; Dolg, M.; Stoll, H.; Preuß, H. Energy-Adjusted Ab Initio Pseudopotentials for the Second and Third Row Transition Elements. *Theor. Chim. Acta* **1990**, *77*, 123–141.
- (34) Dolg, M.; Wedig, U.; Stoll, H.; Preuss, H. Energy-adjusted Ab Initio Pseudopotentials for the First Row Transition Elements. *J. Chem. Phys.* **1987**, *86*, 866–872.
- (35) Martin, J. M. L.; Sundermann, A. Correlation Consistent Valence Basis Sets for Use with the Stuttgart–Dresden–Bonn Relativistic Effective Core Potentials: The Atoms Ga–Kr and In–Xe. J. Chem. Phys. 2001, 114, 3408–3420.
- (36) Marenich, A. V.; Cramer, C. J.; Truhlar, D. G. Universal Solvation Model Based on Solute Electron Density and on a Continuum Model of the Solvent Defined by the Bulk Dielectric Constant and Atomic Surface Tensions. *J. Phys. Chem. B* **2009**, *113*, 6378–6396.
- (37) Grimme, S.; Ehrlich, S.; Goerigk, L. Effect of the Damping Function in Dispersion Corrected Density Functional Theory. *J. Comput. Chem.* **2011**, 32, 1456–1465.
- (38) Glendening, E. D.; Badenhoop, J. K.; Reed, A. E.; Carpenter, J. E.; Bohmann, J. A.; Morales, C. M.; Landis, C. R.; Weinhold, F. In *NBO*, 6.0, Theoretical Chemistry Institute, University of Wisconsin, Madison, 2013.
- (39) Douglas, M.; Kroll, N. M. Quantum Electrodynamical Corrections to the Fine Structure of Helium. *Ann. Phys.* **1974**, 82, 89–155.
- (40) Lu, Q.; Peterson, K. A. Correlation Consistent Basis Sets for Lanthanides: The Atoms La-Lu. J. Chem. Phys. **2016**, 145 (5), 054111.
- (41) Balabanov, N. B.; Peterson, K. A. Systematically Convergent Basis Sets for Transition Metals. I. All-Electron Correlation Consistent Basis Sets for the 3d Elements Sc–Zn. *J. Chem. Phys.* **2005**, 123, No. 064107.
- (42) Bader, R. F. W. Atoms in Molecules. Acc. Chem. Res. 1985, 18, 9-15.
- (43) Bader, R. F. W. A Quantum Theory of Molecular Structure and Its Applications. *Chem. Rev.* **1991**, *91*, 893–928.
- (44) Keith, T. A. In AIMAll, version 17.01.25, TK Gristmill Software, Overland Park KS, 2017.
- (45) Van Lenthe, E.; Baerends, E. J. Optimized Slater-Type Basis Sets for the Elements 1-118. *J. Comput. Chem.* **2003**, 24, 1142–1156.
- (46) te Velde, G.; Bickelhaupt, F. M.; Baerends, E. J.; Fonseca Guerra, C.; van Gisbergen, S. J. A.; Snijders, J. G.; Ziegler, T. Chemistry with ADF. *J. Comput. Chem.* **2001**, *22*, 931–967.
- (47) ADF 2017.106, SCM, Theoretical Chemistry, Vrije Universiteit, Amsterdam: The Netherlands, http://www.scm.com.
- (48) Neese, F. Software Update: The ORCA Program System, Version 4.0. WIREs Comput. Mol. Sci. 2018, 8, No. e1327.
- (49) Pantazis, D. A.; Neese, F. All-Electron Scalar Relativistic Basis Sets for the Lanthanides. *J. Chem. Theory Comput.* **2009**, *5*, 2229–2238
- (50) Ahlrichs, R.; May, K. Contracted All-Electron Gaussian Basis Sets for Atoms Rb to Xe. Phys. Chem. Chem. Phys. 2000, 2, 943-945.
- (51) Weigend, F.; Ahlrichs, R. Balanced Basis Sets of Split Valence, Triple Zeta Valence and Quadruple Zeta Valence Quality for H to Rn: Design and Assessment of Accuracy. *Phys. Chem. Chem. Phys.* **2005**, *7*, No. 3297.
- (52) Karraker, D. G. Coordination of Trivalent Lanthanide Ions. *J. Chem. Educ.* **1970**, *47*, No. 424.
- (53) Lee, C.; Yang, W.; Parr, R. G. Development of the Colle-Salvetti Correlation-Energy Formula into a Functional of the Electron Density. *Phys. Rev. B* **1988**, *37*, 785–789.
- (54) Becke, A. D. Density-functional Thermochemistry. III. The Role of Exact Exchange. J. Chem. Phys. 1993, 98, 5648-5652.

(55) Chai, J.-D.; Head-Gordon, M. Long-Range Corrected Hybrid Density Functionals with Damped Atom—Atom Dispersion Corrections. *Phys. Chem. Chem. Phys.* **2008**, *10*, No. 6615.

- (56) Zhao, Y.; Truhlar, D. G. The M06 Suite of Density Functionals for Main Group Thermochemistry, Thermochemical Kinetics, Noncovalent Interactions, Excited States, and Transition Elements: Two New Functionals and Systematic Testing of Four M06-Class Functionals and 12 Other Functionals. *Theor. Chem. Acc.* 2008, 120, 215–241.
- (57) Peverati, R.; Truhlar, D. G. Screened-Exchange Density Functionals with Broad Accuracy for Chemistry and Solid-State Physics. *Phys. Chem. Chem. Phys.* **2012**, *14*, No. 16187.
- (58) Jerabek, P.; Schwerdtfeger, P.; Frenking, G. Dative and Electron-Sharing Bonding in Transition Metal Compounds: Dative and Electron-Sharing Bonding in Transition Metal Compounds. *J. Comput. Chem.* **2019**, *40*, 247–264.
- (59) Morokuma, K.; Kitaura, K. Energy Decomposition Analysis of Molecular Interactions. In *Chemical Applications of Atomic and Molecular Electrostatic Potentials*; Politzer, P.; Truhlar, D. G., Eds.; Springer US, Boston, MA, 1981; pp 215–242.
- (60) Shahbazian, S. Why Bond Critical Points Are Not "Bond" Critical Points. Chem. Eur. J. 2018, 24, 5401-5405.
- (61) Shaik, S.; Danovich, D.; Silvi, B.; Lauvergnat, D. L.; Hiberty, P. C. Charge-Shift Bonding—A Class of Electron-Pair Bonds That Emerges from Valence Bond Theory and Is Supported by the Electron Localization Function Approach. *Chem. Eur. J.* **2005**, *11*, 6358–6371.
- (62) Shaik, S.; Danovich, D.; Wu, W.; Hiberty, P. C. Charge-Shift Bonding and Its Manifestations in Chemistry. *Nat. Chem.* **2009**, *1*, 443–449.
- (63) Shaik, S.; Danovich, D.; Galbraith, J. M.; Braïda, B.; Wu, W.; Hiberty, P. C. Charge-Shift Bonding: A New and Unique Form of Bonding. *Angew. Chem., Int. Ed.* **2020**, *59*, 984–1001.
- (64) Joy, J.; Danovich, D.; Kaupp, M.; Shaik, S. Covalent vs Charge-Shift Nature of the Metal-Metal Bond in Transition Metal Complexes: A Unified Understanding. *J. Am. Chem. Soc.* **2020**, *142*, 12277–12287.
- (65) Fradera, X.; Austen, M. A.; Bader, R. F. W. The Lewis Model and Beyond. *J. Phys. Chem. A* **1999**, *103*, 304–314.